Publication Year	2016
Acceptance in OA	2020-06-17T14:57:59Z
Title	Geomorphological mapping of comet 67P/Churyumov-Gerasimenko's Southern hemisphere
Authors	Lee, Jui-Chi, MASSIRONI, MATTEO, Ip, Wing-Huen, GIACOMINI, LORENZA, FERRARI, SABRINA, PENASA, LUCA, El-Maarry, Mohamed Ramy, PAJOLA, MAURIZIO, Lai, Ian-Lin, Lin, Zhong-Yi, Ferri, Francesca, Sierks, Holger, Barbieri, Cesare, Lamy, Philippe, Rodrigo, Rafael, Koschny, Detlef, Rickman, Hans, Keller, Horst Uwe, Agarwal, Jessica, A'Hearn, Michael F., Barucci, Maria Antonella, Bertaux, Jean-Loup, BERTINI, IVANO, CREMONESE, Gabriele, Da Deppo, Vania, Davidsson, Björn, Debei, Stefano, De Cecco, Mariolino, Deller, Jakob, FORNASIER, SONIA, FULLE, Marco, Groussin, Olivier, Gutiérrez, Pedro J., Güttler, Carsten, Hofmann, Marc, Hviid, Stubbe F., Jorda, Laurent, Knollenberg, Jörg, Kovacs, Gabor, Kramm, J. -Rainer, Kührt, Ekkehard, Küppers, Michael, Lara, Luisa M., Lazzarin, Monica, MARZARI, FRANCESCO, Lopez Moreno, Josè J., Naletto, Giampiero, Oklay, Nilda, Shi, Xian, Thomas, Nicolas, TUBIANA, Cecilia, Vincent, Jean-Baptiste
Publisher's version (DOI)	10.1093/mnras/stx450
Handle	http://hdl.handle.net/20.500.12386/26112
Journal	MONTHLY NOTICES OF THE ROYAL ASTRONOMICAL SOCIETY
Volume	462

Monthly Notices
of the
ROYAL ASTRONOMICAL SOCIETY

MNRAS **462,** S573–S592 (2016)
Advance Access publication 2017 February 23

doi:10.1093/mnras/stx450

Geomorphological mapping of comet 67P/Churyumov–Gerasimenko's Southern hemisphere

Jui-Chi Lee,[1⋆] Matteo Massironi,[2,3⋆] Wing-Huen Ip,[4,5,6⋆] Lorenza Giacomini,[2] Sabrina Ferrari,[3] Luca Penasa,[3] Mohamed Ramy El-Maarry,[7] Maurizio Pajola,[3,8] Ian-Lin Lai,[5] Zhong-Yi Lin,[4] Francesca Ferri,[3] Holger Sierks,[9] Cesare Barbieri,[10] Philippe Lamy,[11] Rafael Rodrigo,[12,13] Detlef Koschny,[14] Hans Rickman,[15,16] Horst Uwe Keller,[17] Jessica Agarwal,[9] Michael F. A'Hearn,[9,18,19] Maria Antonella Barucci,[20] Jean-Loup Bertaux,[20] Ivano Bertini,[3] Gabriele Cremonese,[21] Vania Da Deppo,[22] Björn Davidsson,[23] Stefano Debei,[24] Mariolino De Cecco,[25] Jakob Deller,[9] Sonia Fornasier,[20] Marco Fulle,[26] Olivier Groussin,[11] Pedro J. Gutiérrez,[27] Carsten Güttler,[9] Marc Hofmann,[9] Stubbe F. Hviid,[9,28] Laurent Jorda,[11] Jörg Knollenberg,[28] Gabor Kovacs,[9] J.-Rainer Kramm,[9] Ekkehard Kührt,[28] Michael Küppers,[29] Luisa M. Lara,[27] Monica Lazzarin,[10] Francesco Marzari,[10] Josè J. Lopez Moreno,[27] Giampiero Naletto,[30] Nilda Oklay,[9] Xian Shi,[9] Nicolas Thomas,[4] Cecilia Tubiana[9] and Jean-Baptiste Vincent[9]

Affiliations are listed at the end of the paper

Accepted 2017 February 20. Received 2017 January 25; in original form 2016 July 5

ABSTRACT

In 2015 May, the Southern hemisphere of comet 67P/Churyumov–Gerasimenko became visible by the *OSIRIS* cameras on-board the *Rosetta* spacecraft. The resolution was high enough to carry out a detailed analysis of the surface morphology, which is quite different from the Northern hemisphere. Previous works show that fine particle deposits are the most extensive geological unit in the Northern hemisphere. In contrast, the Southern hemisphere is dominated by outcropping consolidated terrain. In this work, we provide geomorphological maps of the Southern hemisphere with the distinction of both geological units and linear features. The geomorphological maps described in this study allow us to gain a better understanding of the processes shaping the comet nucleus and the distribution of primary structures such as fractures and strata.

Key words: methods: observational – comets: general – comets: individual: comet 67P/Churyumov–Gerasimenko.

1 INTRODUCTION

Comets belong to the class of the most primitive bodies of the Solar system. Their composition, surface morphology and interior structure can yield key information on planetary formation processes. After its rendezvous with comet 67P/Churyumov–Gerasimenko (C–G) on 2014 August 6, the *Rosetta* spacecraft carried out close-up observations of the nucleus and coma of this Jupiter family comet. The scientific imaging camera system on-board the *Rosetta* spacecraft (Keller et al. 2007), *OSIRIS*, which consisted of a narrow-angle camera (NAC) and a wide-angle camera, made detailed investigations of the physical properties and surface morphology of the comet (El-Maarry et al. 2015a; Groussin et al. 2015; Sierks et al. 2015; Thomas et al. 2015a; Vincent et al. 2015, 2016; Ip et al. 2016; Jorda et al. 2016).

The comet has been subdivided into 26 regions mainly on the basis of clearly visible physiographic boundaries (El-Maarry et al. 2015a, 2016). However, regional physiographic classification is different from geomorphological mapping. In the latter case, the geological units and linear features (strata, scarps and fractures) are

⋆ E-mail: jclee@g.ncu.edu.tw (J-CL); matteo.massironi@unipd.it (MM); wingip@gm.astro.ncu.edu.tw (W-HI)

© 2017 The Authors
Published by Oxford University Press on behalf of the Royal Astronomical Society

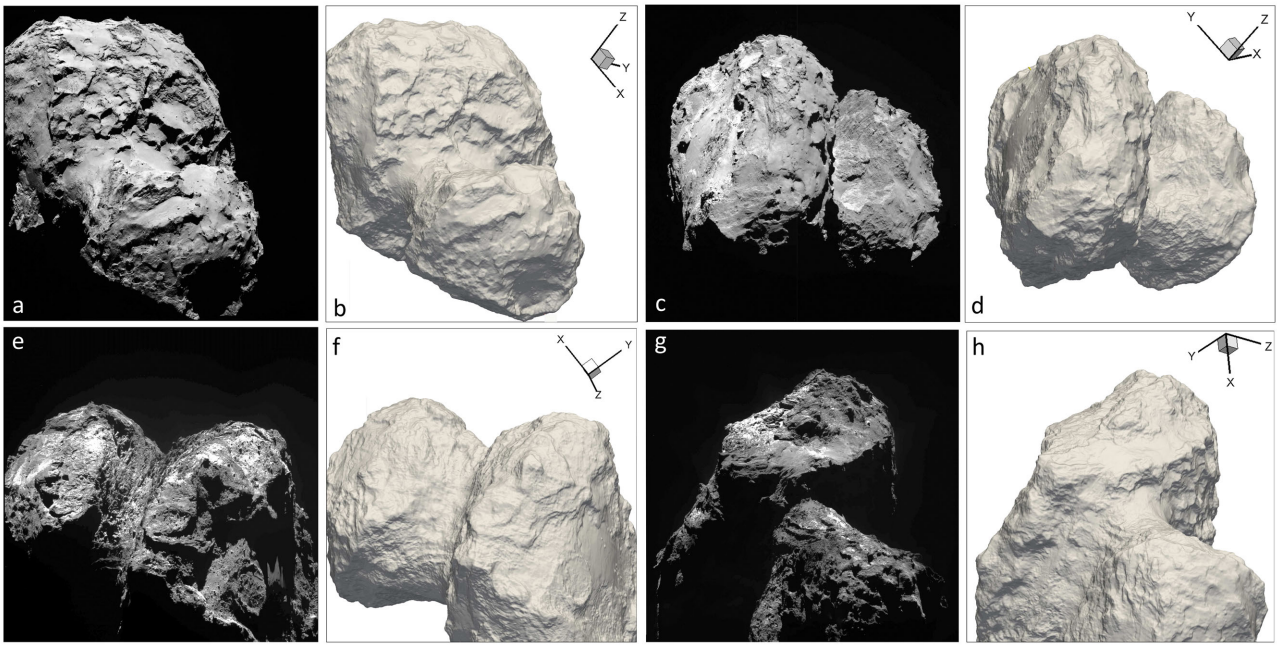

Figure 1. The morphological diversity between the Northern (a–d) and Southern hemispheres (e–h). (a),(c),(e),(g) are the NAC images taken by *OSIRIS* camera; (b),(d),(f),(h) are the corresponding shape models in the same orientation as the image on the left-hand side.

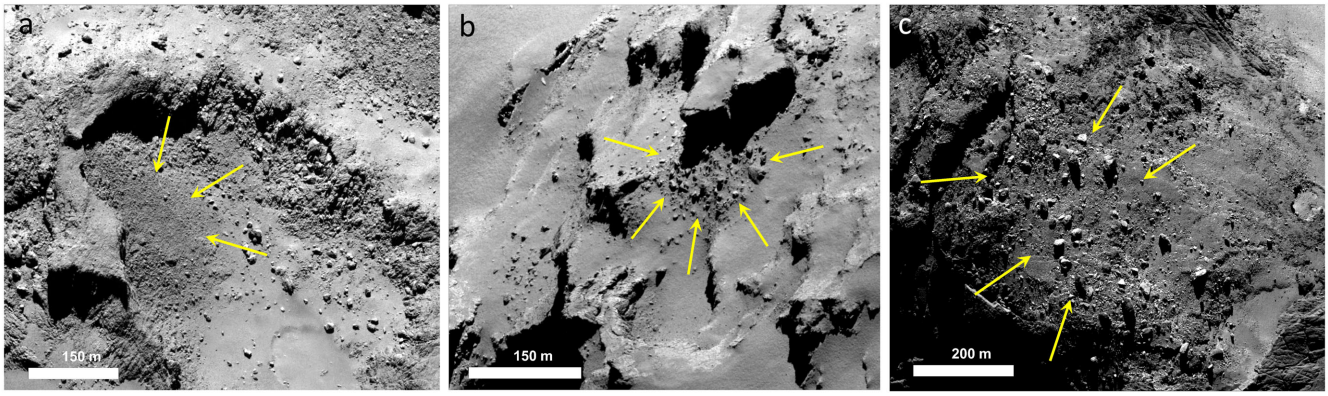

Figure 2. Examples of mass wasting deposits. (a) Yellow arrows indicate the talus deposits at the foot of a cliff. (b) Gravitational accumulation deposits are composed of boulders and blocks from 2 to 30 m. (c) The diamicton is composed of poorly sorted deposits that can be even further from cliffs.

classified on the basis of their geomorphological properties as well as their probable origins. For this reason, a single geological unit or linear feature is not limited to a given physiographic region.

The Southern hemisphere of the nucleus surface reveals quite different morphologies from the northern one (Fig. 1). This work presents the first geomorphological maps of the Southern hemisphere in which linear features and geological units are reported, which is a companion paper to Giacomini et al. (2016). Their work presented the first geomorphological maps of the Northern hemisphere using the NAC images of 2014 August and September. In this way, we can compare the geomorphology between the Northern and Southern hemispheres of comet 67P interpreting the possible reasons for the observed differences.

2 METHODOLOGY AND DATA SET

To perform the geomorphological mapping, we used the images taken by the NAC of the *OSIRIS* imaging system (Table A1). On the basis of surface textures and morphologies, we have classified the nucleus surface into different geological units, as in La Forgia et al. (2015), Giacomini et al. (2016) and Pajola et al. (2016b). In particular, we have distinguished rocky outcrops and non-cohesive deposits. Among the latter, the mass wasting deposits (La Forgia et al. 2015; Pajola et al. 2015), probably generated by concurrent processes of sublimation and gravitational collapses (Pajola et al. 2015), can be classified into three types using the same classification scheme as reported in Giacomini et al. (2016):

(1) Talus: deposits whose particle diameters are from 2 to 18 m lying on slopes underneath steep scarps (Fig. 2a).
(2) Gravitational accumulation deposits: poorly sorted deposits ranging from 2 to 30 m close to the feet of scarps (Fig. 2b).
(3) Diamicton: highly heterogeneous deposits of uncertain origin (Fig. 2c).

There are also homogeneous fine particle deposits that might be the result of airfalls (Thomas et al. 2015a,b; Keller et al. 2015; Lai et al. 2017). The 'fine particle deposits' has been resolved as cm-sized debris by the ROLIS instrument on Philae at the landing

Table 1. Definition of the geological units.

Types of material		Mapping terms	Description
Consolidated material		Outcropping consolidated terrain	Rocky terrain without non-cohesive deposits.
		Isolated blocks	Blocks larger than 18 m and unrelated to any specific deposits or sources.
Non-cohesive deposits	Mass wasting deposits	Talus	Deposits with particle diameters ranging from 2 to 18 m.
		Gravitational accumulation deposits	Deposits with block diameters ranging from 2 to 30 m and attributed to gravitational collapses.
		Diamicton	Heterogeneous and poorly sorted deposits of uncertain origin.
	Fine material	Fine particle deposits	Homogeneous fine particles resolved as cm-sized debris by the ROLIS instrument.
		Smooth plain	Smooth deposits showing no roughness with surface texture smoother than fine particle deposits.

Table 2. Definition of the linear features.

Types of features		Mapping terms	Description
Primary features	Stratification	Terraces/Cuestas	Topmost layer of stratification. Asymmetric morphologies showing a steep slope on one side and a plane with a gentle dip (cuestas) or no dip (terraces) on the other side.
		Strata	Parallel linear features resulting from the intersection of layers with the topography aligned with denudation terrace margins and cuesta ridges, often associated with terraces organized in a staircase pattern.
		Fractures	Cracks of variable lengths on consolidated materials.
Evolutionary features		Pit margins	Semi-circular or circular scarps produced by the erosion of the pit wall.
		Niches	Remnants of the pits or crown areas of rockfalls.
		Scarps	Steep walls caused by cliff collapses and retreat events.

site (Mottola et al. 2015). We identify the unit as 'smooth plain' when the surface texture is smoother than fine particle deposits. Solid particles larger than cm-size are transported by outgassing events or outbursts, while smaller ones are produced by airfall mechanisms (Thomas et al. 2015a; Lai et al. 2017). A new geological feature, 'isolated blocks' (Bruno & Ruban 2017), is also identified. These are blocks larger than 18 m that are apparently unrelated to any specific deposit or source. They are interpreted as leftovers of erosive sublimation events of pre-exist terrain or as 'erratic' blocks moved under gravity control. A summary of the geological units we defined is given in Table 1.

We have also mapped several linear features. In addition to the four kinds of linear features defined by Giacomini et al. (2016) in the Northern hemisphere (cuesta margins, strata, fractures, niches), we identified scarps and pit margins. Therefore, we classified the linear features into six types (Table 2) as follows:

(1) Strata: We classified 'strata' as the traces produced by the intersection of bedding planes with the topography (as in Giacomini et al. 2016). Strata are observed on cliffs as parallel linear features usually in alignment with cuesta ridges and terrace margins that are often repeated in staircase patterns (white arrows in Fig. 3a, Auger et al. 2015; La Forgia et al. 2015; Pajola et al. 2015; Rickman et al. 2015; Vincent et al. 2015; Feller et al. 2016; Giacomini et al. 2016; Ip et al. 2016). The strata can be used to interpret the internal structure of the comet (Massironi et al. 2015).

(2) Terraces/Cuestas: Terraces are flat planes limited by subvertical cliffs, whereas cuestas are asymmetric landforms with a steep slope on one side and a gentle slope on the other. The boundary between the flat plane and the subvertical cliff is called the terrace margin, and the limit between the two different slopes of a cuesta is named the cuesta ridge. Denudation terraces and cuestas are, by definition, landforms modelled by erosive processes on stratified material. Both forms derive from differential erosion, where a harder layer overlays a weaker one (yellow arrows in Fig. 3a; see Thornbury 1954; Fairbridge 1968; Summerfield 1991; Ahnert 1998; Easterbrook 1993; Bierman & Montgomery 2014). Auger et al. (2015), Vincent et al. (2015) and Pajola et al. (2016a) describe erosion and the retreat of cometary cliffs on 67P leading to the formation of denudation terraces, whereas Auger et al. (2015), Massironi et al. (2015) and Giacomini et al. (2016) describe cuesta morphologies at many other locations of the nucleus. Both morphologies are, hence, an expression of stratification, where the gentle or non-dipping planes define the orientation of the stratification on that location. The lines traced within the map follow the terrace margins or the cuestas ridges.

(3) Fractures: Fractures are cracks of variable length on the consolidated material (yellow arrows in Fig. 3b). Several kinds of fractures have been observed on comet 67P (El-Maarry et al. 2015b). These include: polygonal fracture networks, fractured cliffs, fractured boulders and isolated fractures. Differently from the strata, they are not joined to any terrace margins or cuesta ridges, and they are often arranged in conjugate and anastomosing sets or in en-echelon geometries. In Fig. 3(b), we show one kind of fractures as an example. The possible formation mechanisms for most of them are thermal shock and/or thermal fatigue (El-Maarry et al. 2015b; Thomas et al. 2015a) although some can be caused by orbital-induced or tidal-like forces and impacts (El-Maarry et al. 2015b; Pajola et al. 2016b).

(4) Pit margins: Being the more peculiar features, 'pit margins' are semi-circular or circular scarps produced by erosion of the pit walls (white arrows in Fig. 4a, Vincent et al. 2015). The deposits inside the pits, which we defined as 'pit deposits', are thus composed of fine material that has collapsed and fallen from their walls (yellow arrow in Fig. 4b).

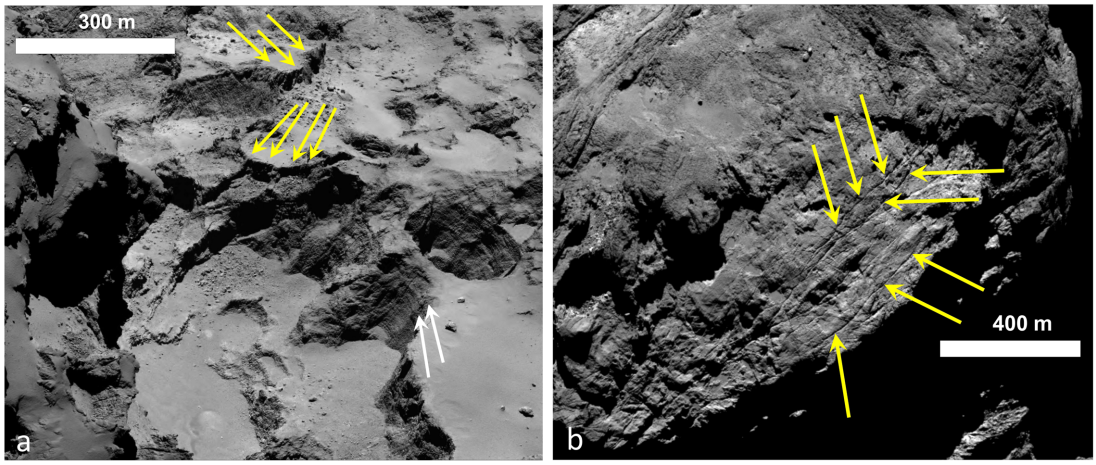

Figure 3. Examples of the linear features. (a) White arrows point out the strata on the cliff, whereas the topmost layer of the strata sequence corresponds to terrace planes and cuestas gentle slopes (yellow arrows). (b) Yellow arrows indicate long fracture systems on Wosret.

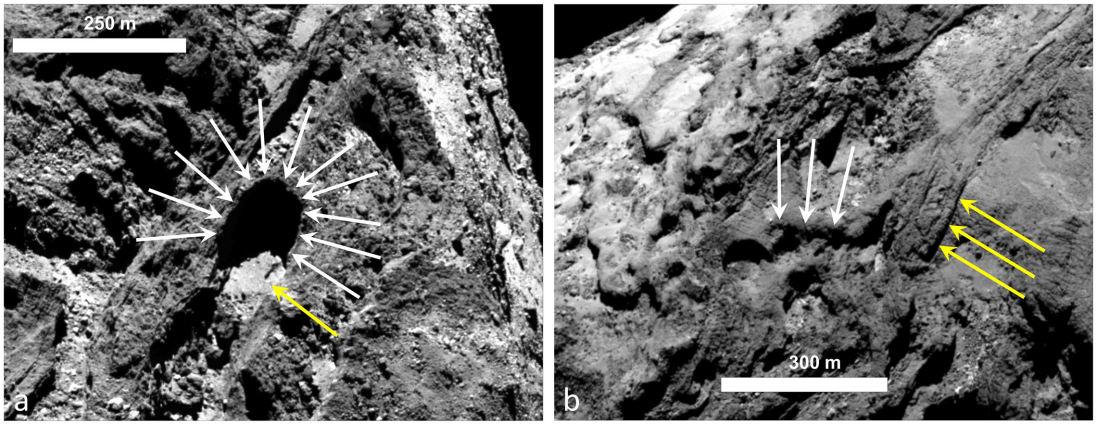

Figure 4. Example of the pit margins and scarps. (a) Half-pit on Anhur: white arrows show the pit margin, whereas the yellow one indicates the pit deposits composed of fine material. (b) Yellow arrows indicate bands of strata on Wosret, while the white arrows indicate some erosional scarps.

(5) Niches: These appear to be quiescent remnants of circular pits or crown areas of gravitational falls.

(6) Scarps: These are steep walls likely caused by cliff collapse and retreat events (white arrows in Fig. 4b).

Strata and fractures are primary structures, while terrace margins, cuesta ridges, pit margins, niches and scarps are evolutionary morphologies that might model the primary structures. Since, on geological maps, linear features must be classified according to the last geological event that shaped them, a linear feature indicating a stratum can become a cuesta ridge, a denudation terrace margin, a pit margin, a niche or a scarp, if the stratum has been modelled by a later erosive process. Similarly, a fracture plane can define a scarp which, in turn, can be modelled by later collapses generating niches.

In the Northern hemisphere, Massironi et al. (2015) derived some interpretative geological sections of the inner nucleus on the basis of the orientation of terrace planes and the gentle slopes of cuestas, given that these morphologies are, by definition, the expression of subsurface stratification. On the basis of such geological sections, they suggested two independent onion-like structures for the two lobes. In this study, we apply the same method by using the stratification observed in both hemispheres to realize three geological sections through comet 67P. As shown in Fig. 5, a reasonable interpretation of the measured strata is given by two onion-like inner structures.

3 GEMORPHOLOGICAL MAPS

We provide eight geomorphological maps for the Southern hemisphere in order to complete the mapping of the entire 67P nucleus surface. Figs 6 and 7 show the images we used together with the regional boundaries outlined by El-Maarry et al. (2016) and the correspondent perspective views of the shape model (Jorda et al. 2016), upon which the longitude and latitude grid in the Cheops reference frame has been projected (Preusker et al. 2015). Fig. A1 shows different perspective views of the shape model on which the visible part of the regions mapped in this work have been projected. The geomorphological maps are presented in Fig. 8 to 15 and, in the next sections, are described following the regional distinctions of El-Maarry et al. (2016).

3.1 Wosret region

The Wosret region, located on the head in the Southern hemisphere, is characterized by outcropping consolidated terrain, with scattered blocks and patches of fine particle deposits. In this region, we have identified six pits with diameters from 45 to 100 m (Fig. 8). One

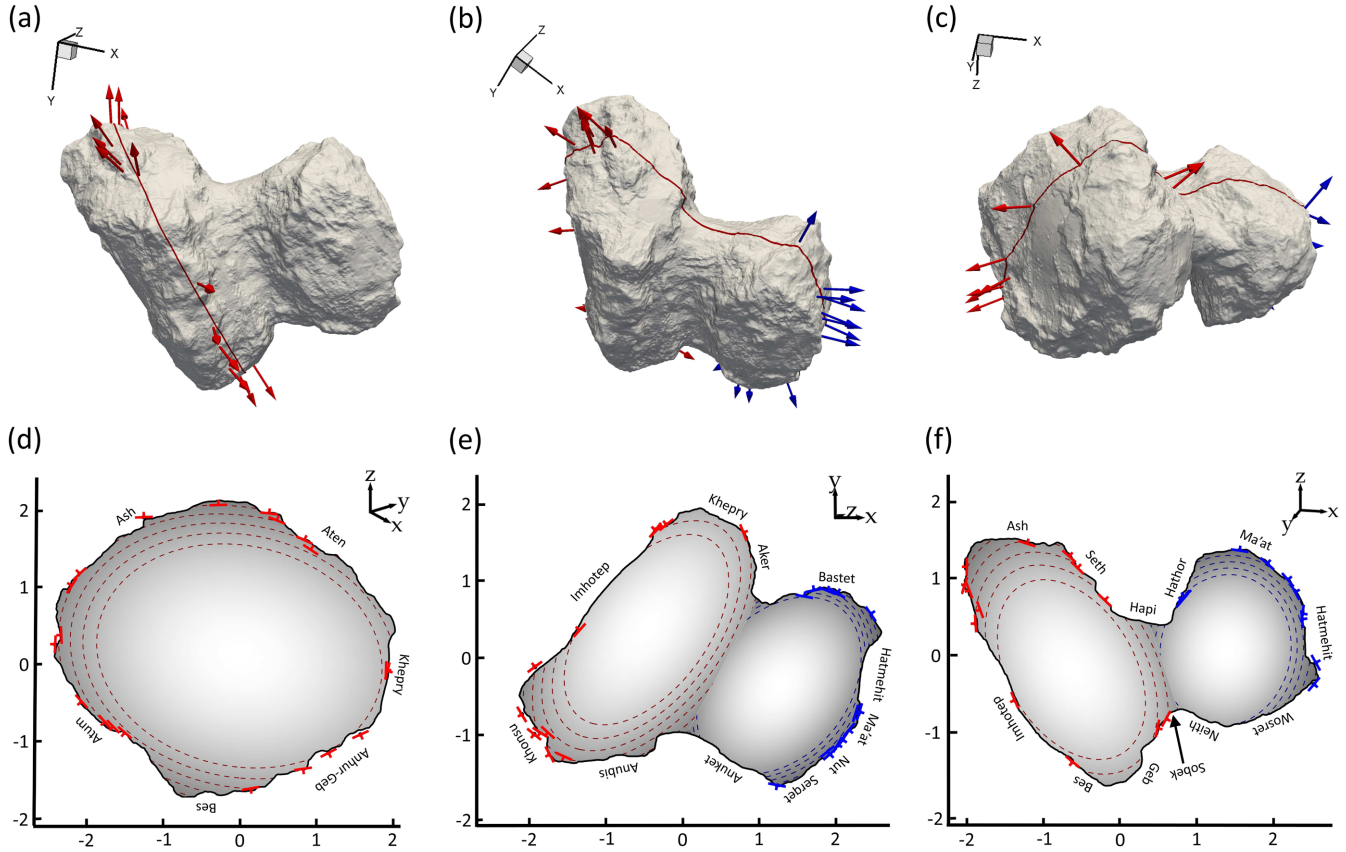

Figure 5. Hypothetical geological sections of the comet. On the upper part, from (a) to (c), the red lines show the intersection of the section plane with the topography. The arrows indicate the estimated normal vectors to the inferred layer in proximity to the section plane. Flat regions, which were interpreted as terraces created by differential erosion, were used as proxies for the local layer orientation. On the lower part, from (d) to (f), the red and blue symbols represent the local orientation of layers on the body and head, respectively. Dashed lines represent an interpretation of the subsurface based on elliptical shells, in which the thickness of the visible layering for the specific section is evenly subdivided into five intervals.

half-pit, close to the Hatmehit region, shows a stratified wall on one side, suggesting that strata are composed of relatively hard material. Several scarps regularly follow the boundary between Wosret and Maftet. At their feet are talus and gravitational accumulation deposits (Figs 8 and 16), which are most probably linked to concurrent erosional and gravitational activities (Vincent et al. 2016).

According to the geological section of Fig. 5, the deeper (inner) shells of the head should be exposed in the central Wosret region. Indeed, Fig. 17(a) of the Wosret region shows three 'bands' of parallel linear features that can be interpreted as strata connected with staircase terraces. The general attitudes of these stratifications suggest a clear envelope of the lobe (Fig. 17b).

3.2 Anhur and Geb

Both Anhur and Geb are characterized by elevated terrains at higher latitudes that downgrade with a sequence of cliff and terraces in a staircase pattern towards a common elongated depression (Fig. 8), where, according to Fig. 5d, the deeper shells of the nucleus' envelopes are exposed. The Geb region is dominated by outcropping consolidated terrain characterized by linear features interpreted as strata and terrace margins. Both linear features continue without any interruption into the Anhur region. Hence, there are no structural reasons to separate the two regions. However, Anhur is richer in blocks, boulders and different kinds of deposits originating from the prominent cliffs (Fig. 8) that likely underwent erosive events by sublimation and gravitational falls (Pajola et al. 2016a; Vincent et al. 2016). Close to the Sobek side is a very thin cover of smooth material unable to hide the strata of the consolidated material underneath. This material could be the product of the global dust transport described by Thomas et al. (2015b) and Lai et al. (2017). Polygonal networks of fractures of variable lengths have been detected on consolidated terrain at the boundary of Anhur and Geb. These features could be related to the weathering effect associated with thermal stress, as described in El-Maarry et al. (2015b).

3.3 Bes region

The Bes region is located at high latitudes of the Southern hemisphere and its geomorphological map is based on two images (Figs 9 and 10). The general geomorphology is characterized by outcropping consolidated terrain covered with deposits of fine materials. Fig. 9 shows how the terraced terrains of the Anhur region extend into Bes. At the feet of the steep cliffs bounding the terraces are diverse deposits. Among them, but located further from the cliffs' base, is a diamicton containing some scattered blocks within a heterogeneous matrix (Pajola et al. 2016a). These deposits could be the result of mass movements towards areas of low gravitational potential (Lai et al. 2017). Alternatively, they can be explained as a deposit of autochthonous remnants of erosional processes.

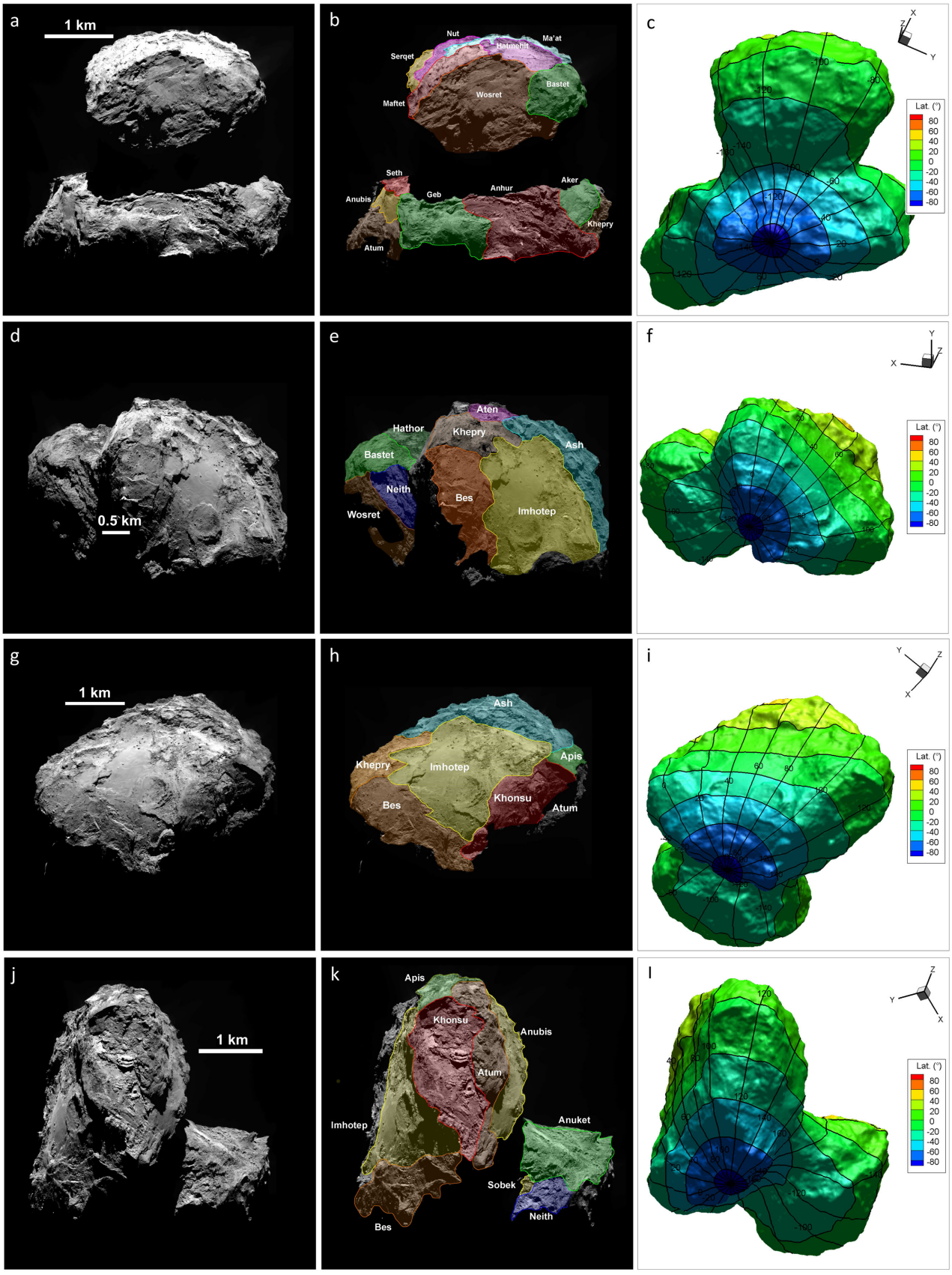

Figure 6. *OSIRIS* images used for maps in Figs 8–11, related regional boundaries and shape model with highlighted longitudes and latitudes.

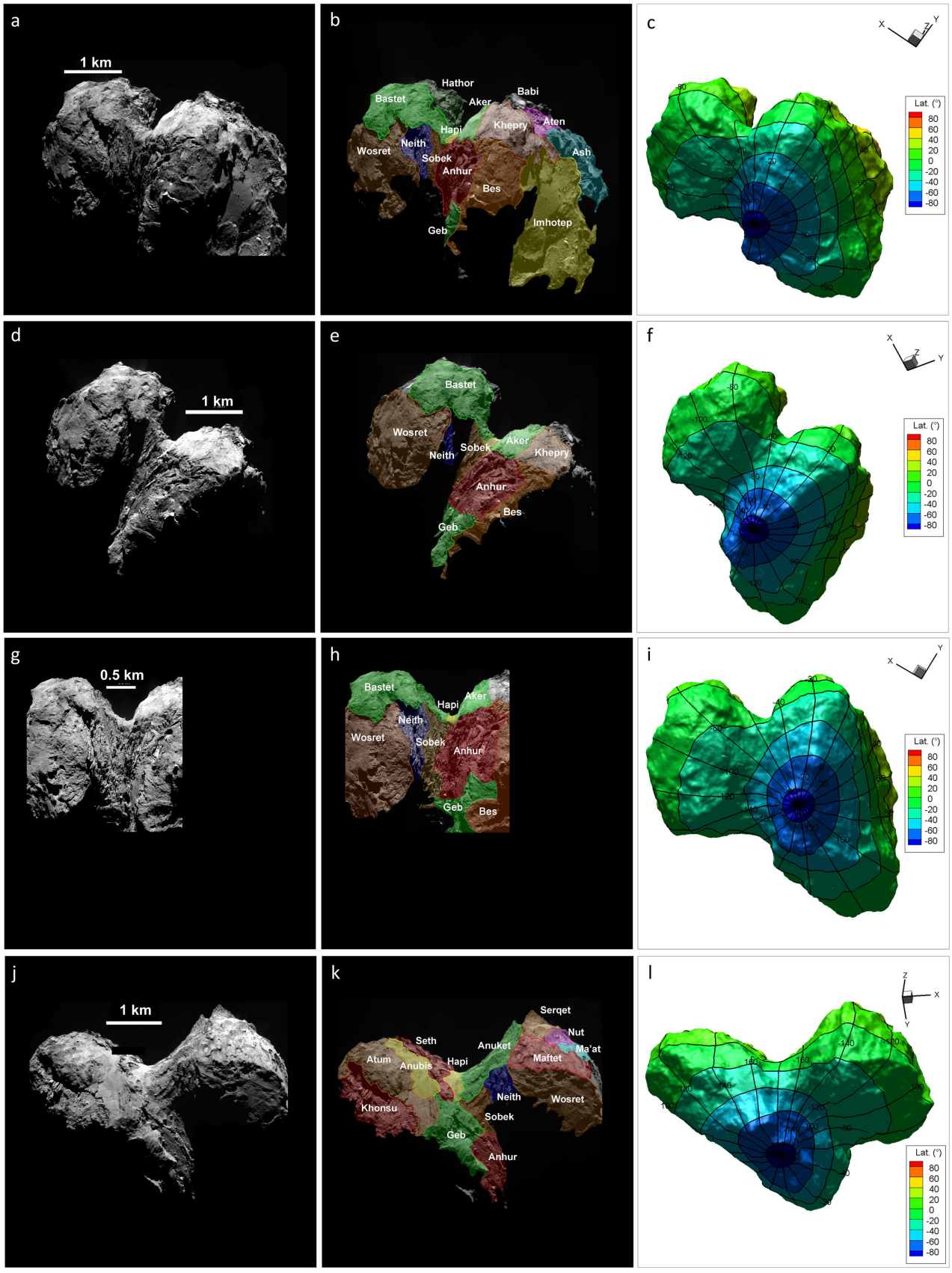

Figure 7. *OSIRIS* images used for maps in Figs 12–15, related regional boundaries and shape model with highlighted longitudes and latitudes.

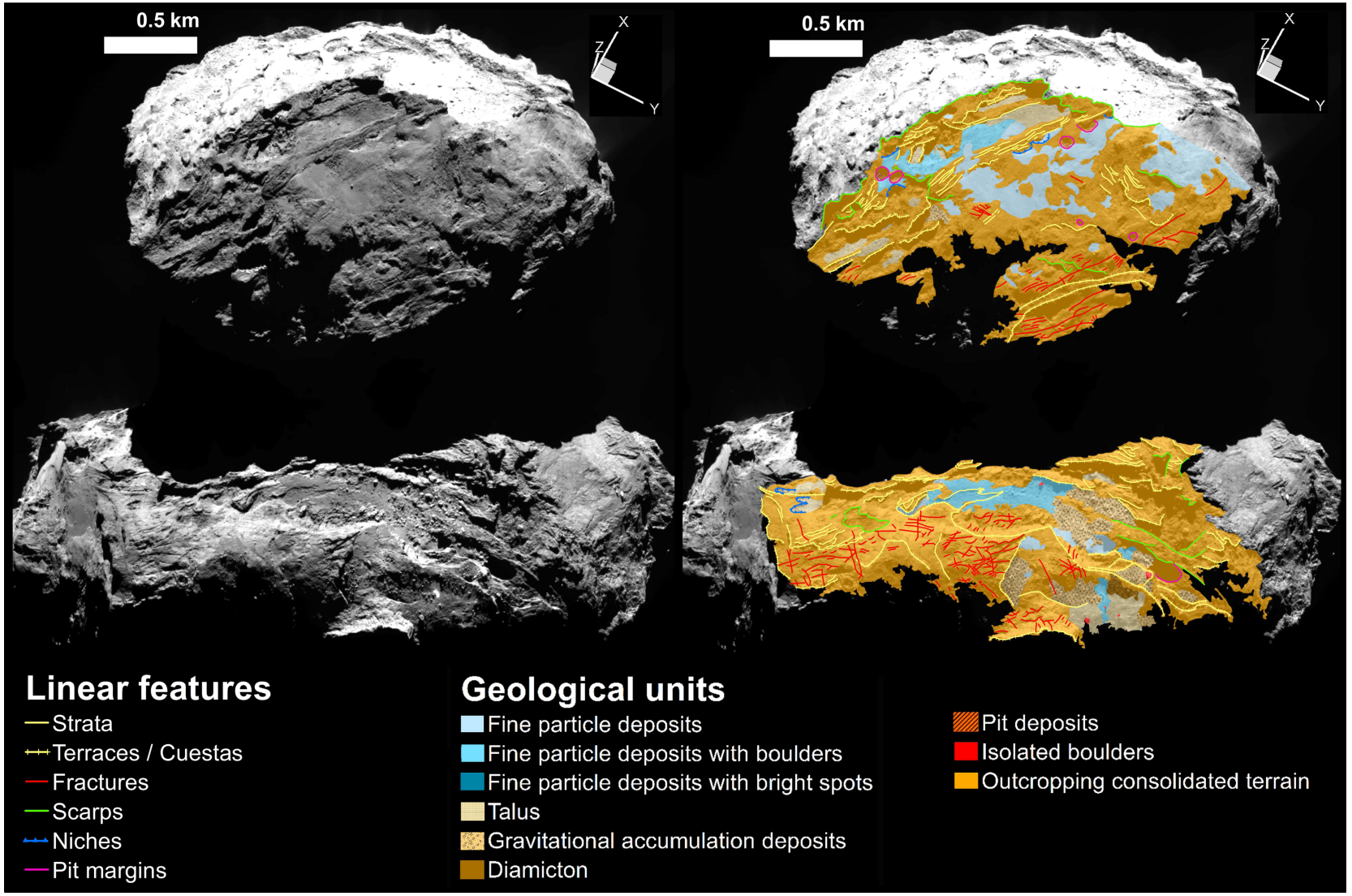

Figure 8. Geomorphological map of Wosret, Geb and Anhur regions.

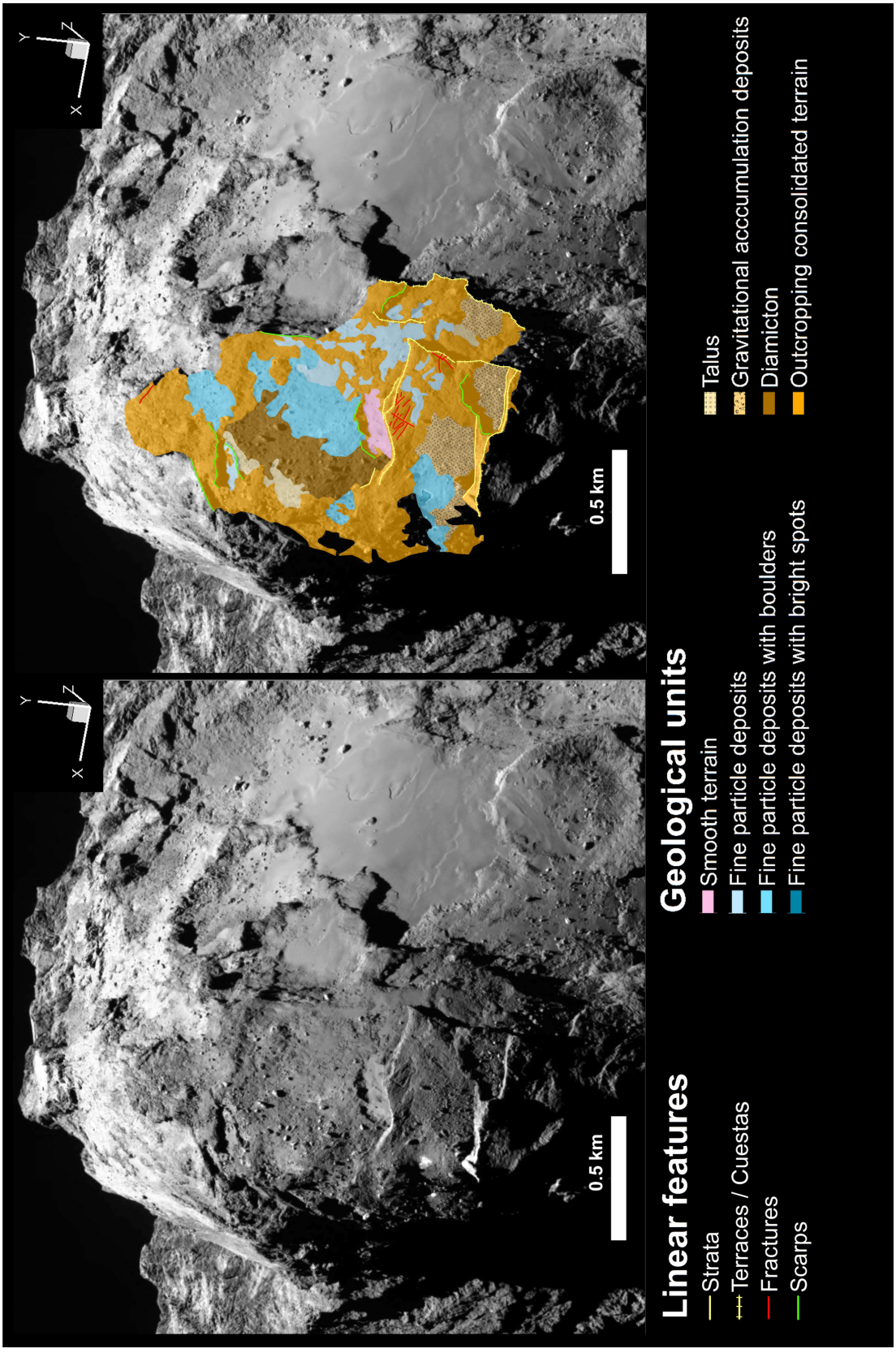

Figure 9. Geomorphological map of Bes region.

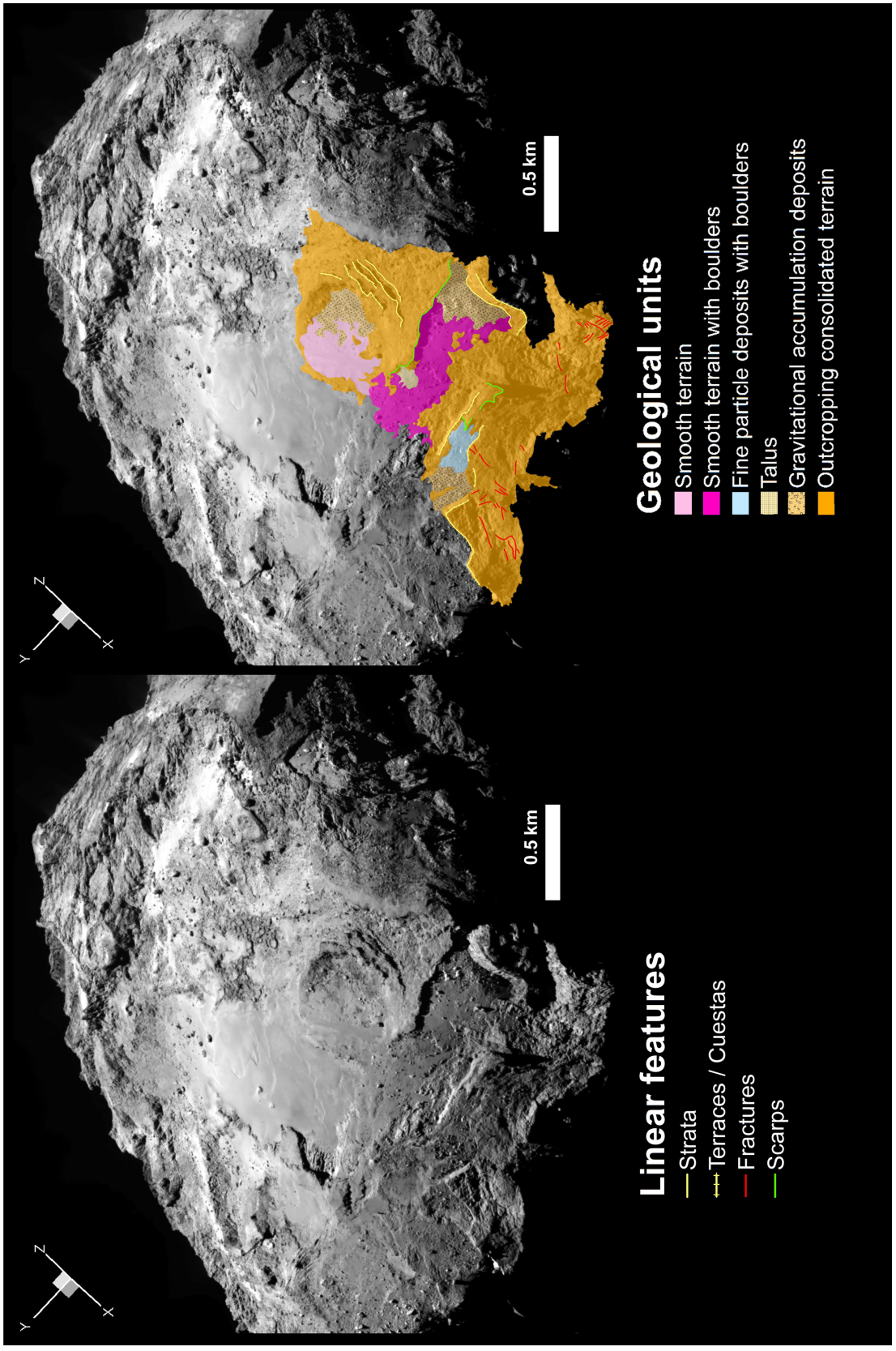

Figure 10. Geomorphological map of Imhotep and Bes regions.

Finally, there is a polygonally fractured surface near a cuesta margin (El-Maarry et al. 2015b, 2016).

3.4 Imhotep

The southern part of Imhotep (Fig. 10) was in shadow in 2014 and, hence, was not mapped by Auger et al. (2015) or Giacomini et al. (2016). The smooth terrain in the centre of Imhotep (and reported by Auger et al. 2015; Giacomini et al. 2016) extends to our region of interest. In the model of Lai et al. (2017), this region should be covered by relatively thick airfall deposits. It is most likely that under the smooth material is the consolidated terrain (Auger et al. 2015; Massironi et al. 2015). Cuestas, terraces and strata can be observed in the regions surrounding Imhotep as shown in Fig. 10. According to the geological section of Figs 5(b) and (c), Imhotep is a window into the deeper layer of the onion-like structure.

3.5 Khonsu region

Khonsu covers a region from equatorial to mid-latitudes of the Southern hemisphere (Fig. 11). It is dominated by outcropping consolidated terrain overlaid by some patches of fine particle deposits. The boundary between the Apis and Khonsu regions is dominated by a 100-m high scarp. A structure defined by a stack of three layers, here called 'pancake outcropping terrain', is at the centre of the region. It seems to be a possible exotic block that might have formed during the accretion process (El-Maarry et al. 2016).

In Fig. 11, the stratification shown in yellow runs through the outcropping consolidated terrain (brown unit) along latitudinal directions, whereas the strata in the bright outcropping terrain (green unit) range nearly along meridians. This can be due to different perspective views of the onion-shell stratification shown in Fig. 5. From the identification of linear features and geological units, we can simply divide this region into two parts. The southern part is made up of bright outcropping material (green unit in Fig. 11) with a more chaotic and fractured sector underneath. The lines in yellow are strata, and the lines in orange are open fractures or 'crevices'. The widths of these crevices range from approximately 5 to 20 m, larger than the fractures we have generally observed on the comet nucleus. Inside the crevices are fine particle deposits (Fig. 18). The origin of the crevices could be fracturing at the merging of the two lobes. This kind of fracturing could have formed only in the inner parts of the comet because the possible unloading in the shallowest sectors of the nucleus is likely lower and could have been completely absorbed by the already existing polygonal framework of fractures generated by thermal fatigue (El-Maarry et al. 2015b). The fine material within and outside the crevices could come from airfall processes (Thomas et al. 2015b). In the global dust transport model calculation of Lai et al. (2017), the Khonsu region should not be rich in airfall deposits, but this is what we actually observe in Fig. 11, where the exposed fresh part of the comet nucleus is mostly composed of consolidated material. As a result, we can infer that the removal of the shallower materials, which led to the exposure of the pancake outcropping terrain, is possibly due to an older collisional event on Khonsu and that the series of crevices did not form recently, since there was sufficient time for patches of fine particles to be deposited in this region.

3.6 Southern hemisphere neck

We use four maps to present the geomorphology of the neck in the Southern hemisphere (Figs 12, 13, 14 and 15). The neck sector contains two regions: the Sobek region, which is located on the neck, and the Neith region, which corresponds to the steep cliffs still pertaining to the head (Fig. 5f, El-Maarry et al. 2016). The general geomorphology of the Neith and Sobek regions can be described as outcropping consolidated terrain with poorly sorted blocks (Pajola et al. 2016a). The fine particle deposits are not as widespread as in the Hapi region in the Northern hemisphere (see Giacomini et al. 2016). Only the centre of Sobek (blue units in Fig. 14) is covered by fine deposits, which might be due to airfall from outgassing activity (Thomas et al. 2015a,b). The blocks could have been transported from the Wosret, Anhur and Bes regions because of the low gravitational potential within the Sobek region (Lai et al. 2017). The strata and cuesta ridges can be seen in the Sobek as well as the Neith regions. The dip of the cuestas' long slopes (i.e. strata) is relatively high, which could be explained by the attitude predicted by the onion-like inner structure of the geological sections of Fig. 5 and/or by the compression generated during the merging of the two separated cometesimals that gave rise to the two lobes (Rickman et al. 2015; Massironi et al. 2015). There are some scarps cutting across the strata in Figs 14 and 15. At the feet of these scarps are gravitational accumulation deposits. We also observed semi-circular niche and terrace margins at the boundary between the neck and the main body (Fig. 15).

4 DISCUSSION

The head of the Northern hemisphere is widely covered by fine particle deposits (El-Maarry et al. 2015a; Thomas et al. 2015b; Giacomini et al. 2016), and only a few regions display consolidated material, like the steep slopes of cuestas and hogbacks in the Ma'at and Maftet regions (La Forgia et al. 2015) and the margins of the large Hatmehit depression. By contrast, in the southern part of the head, Fig. 8 shows widespread outcropping terrain only partly covered by non-cohesive materials, such as airfall deposits and gravitational accumulations.

The neck of the Northern hemisphere is represented by the Hapi region, which is composed of cohesionless material with a row of large blocks at its centre (Pajola et al. 2015; El-Maarry et al. 2015a). A layered outcropping terrain is gradually exposed at the transition region from Hapi to the Southern hemisphere. Indeed, the neck in the Southern hemisphere is dominated by consolidated stratified material (Figs 12, 13 and 14). In this area, only very few patches of non-cohesive materials of different textures are at the base of some scarps.

Most of the Northern hemisphere of the body is characterized by the circular depressions with various diameters and depths that are typical of the Seth region (Ip et al. 2016). All the other regions of the Northern hemisphere are in any case widely covered by fine material with the only exception being several gravitational deposits at cliffs' bases (Groussin et al. 2015; Giacomini et al. 2016). Figs 8 and 11 show the Geb, Anhur and Khonsu regions, which are representative of the Southern hemisphere of the main body. As for the head and neck, the fine deposits in these regions are sparser than in their northern counterparts, being limited to some discontinuous patches of smooth materials within the consolidated terrain. The Khonsu region also displays some unique features, such as crevices and the 'pancake' outcrop.

In summary, the most extensive terrains in the Northern hemisphere are made up of fine particle deposits (Auger et al. 2015; El-Maarry et al. 2015a; Thomas et al. 2015b; Giacomini et al. 2016), while the Southern hemisphere is dominated by outcropping consolidated terrain. In addition, the Northern hemisphere shows a highly

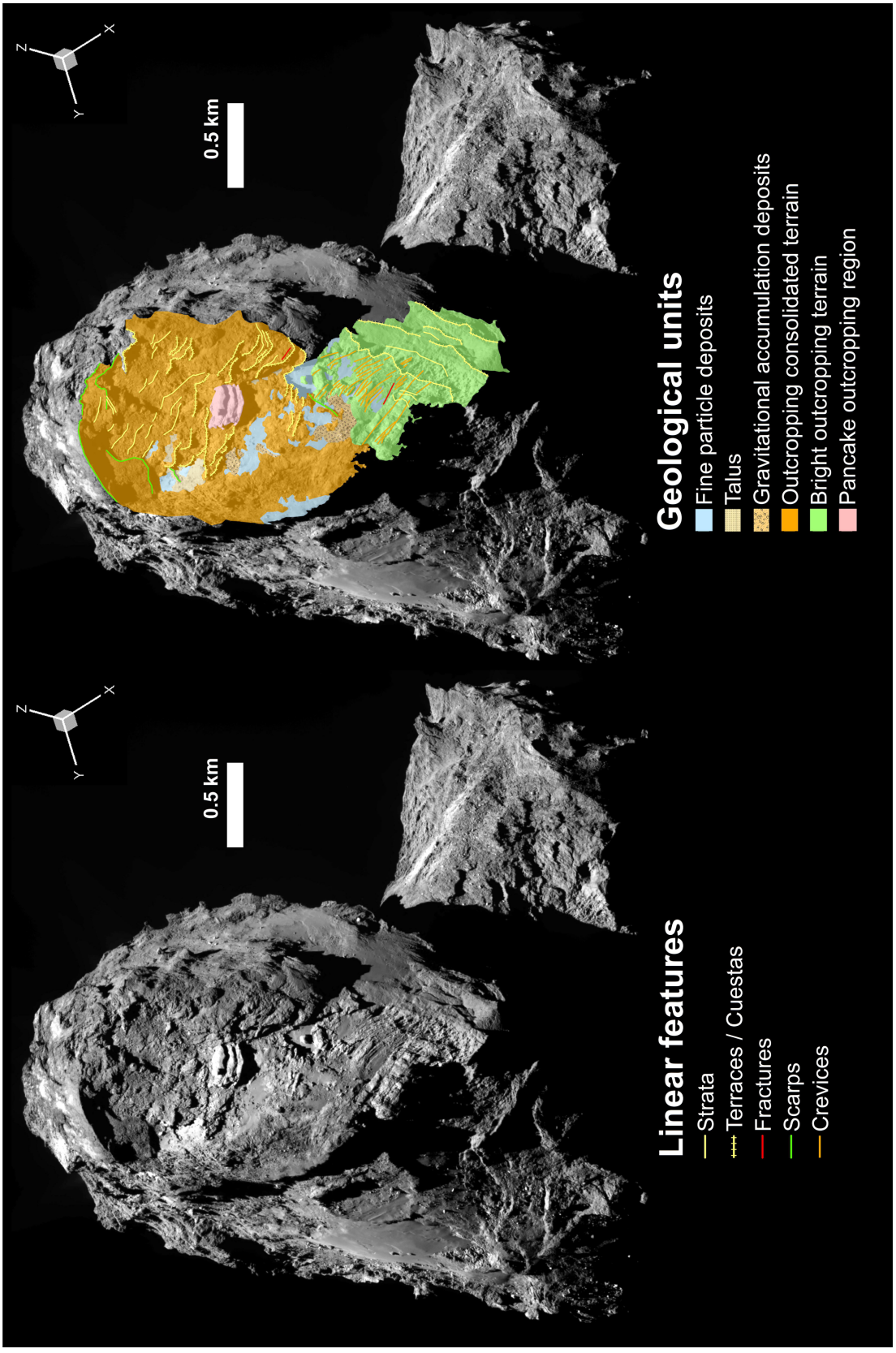

Figure 11. Geomorphological map of Khonsu region.

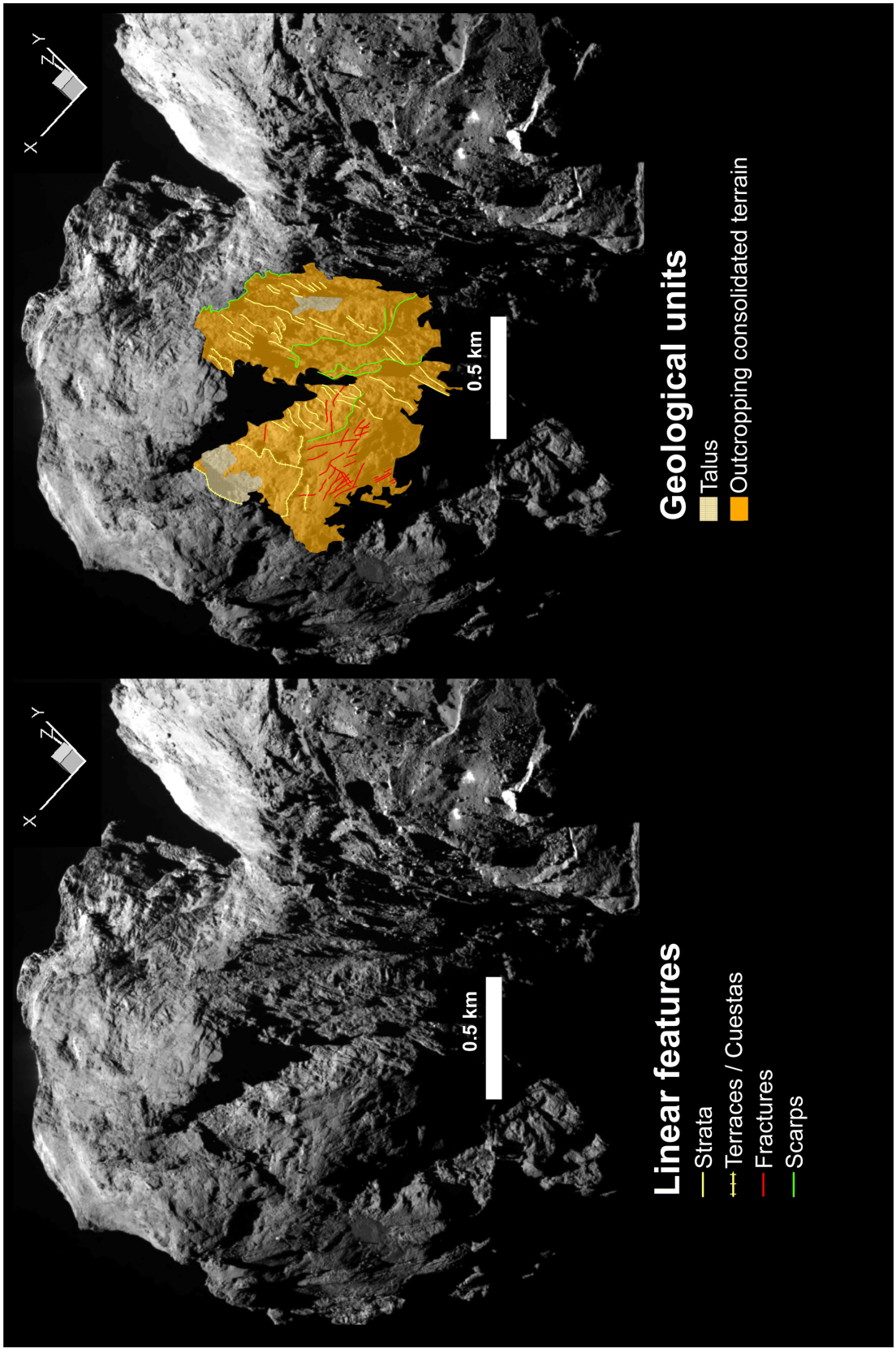

Figure 12. Geomorphological map of Neith region.

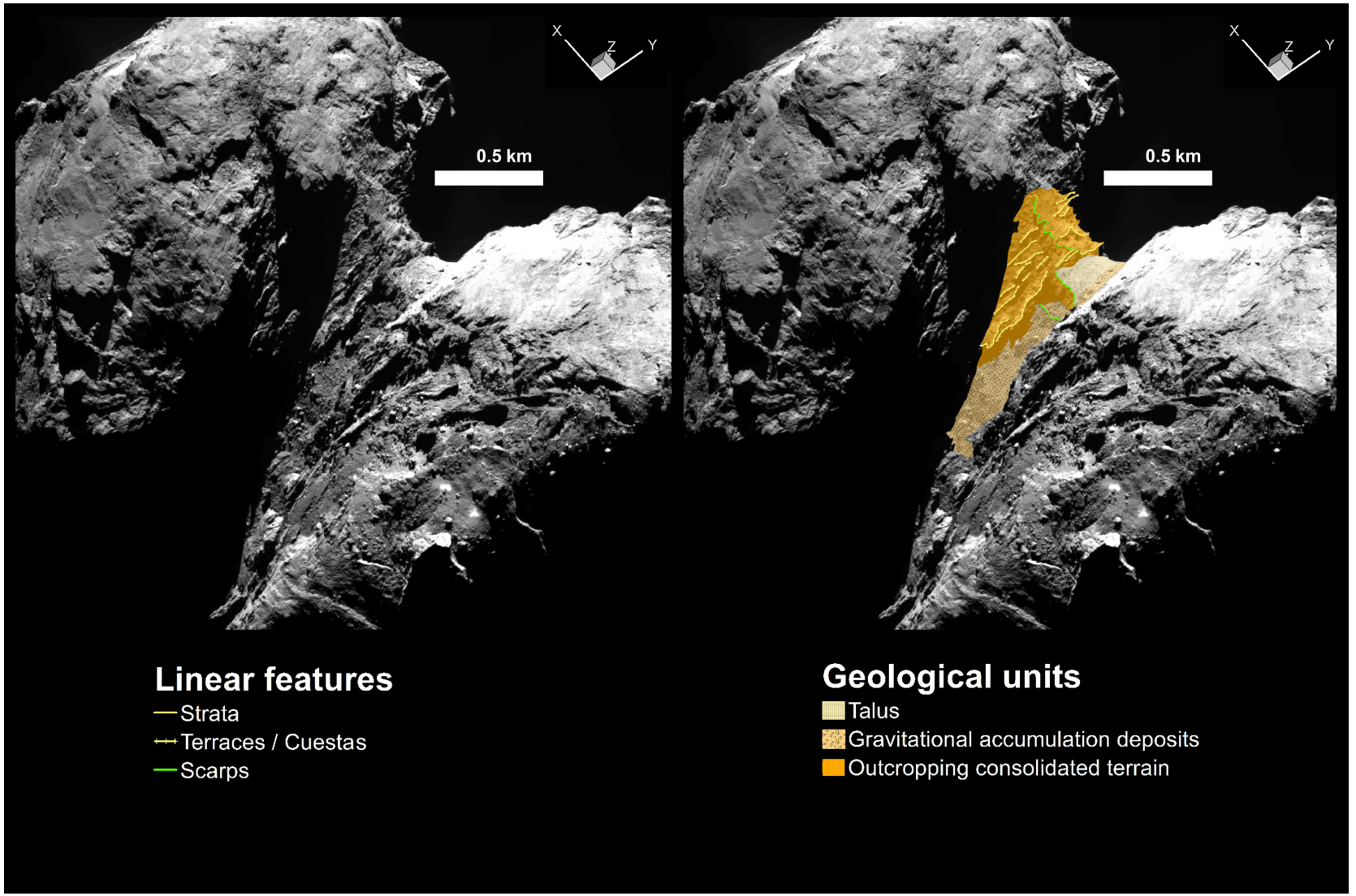

Figure 13. Geomorphological map of Sobek, Neith and Bastet regions.

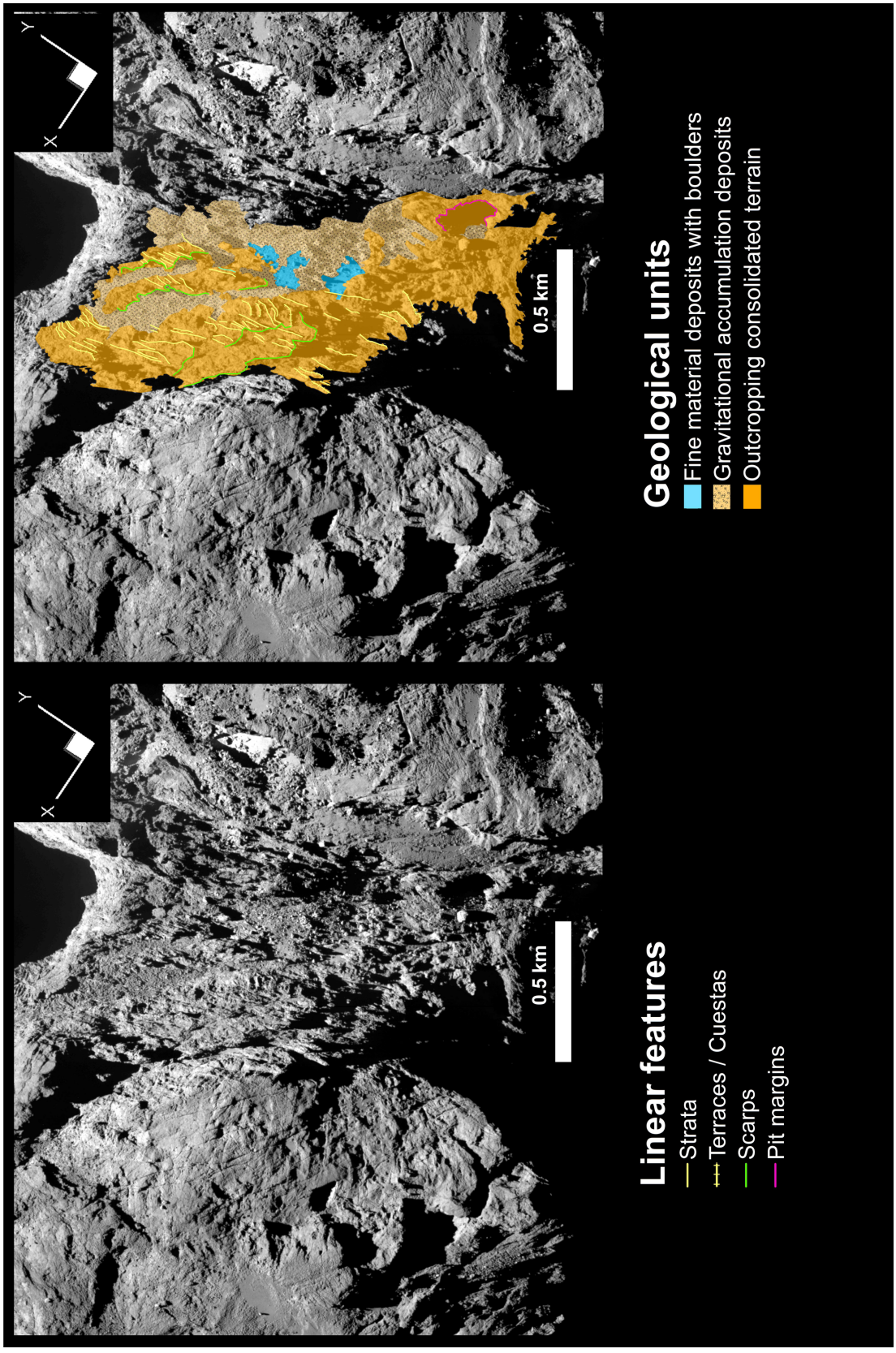

Figure 14. Geomorphological map of Neith and Sobek regions.

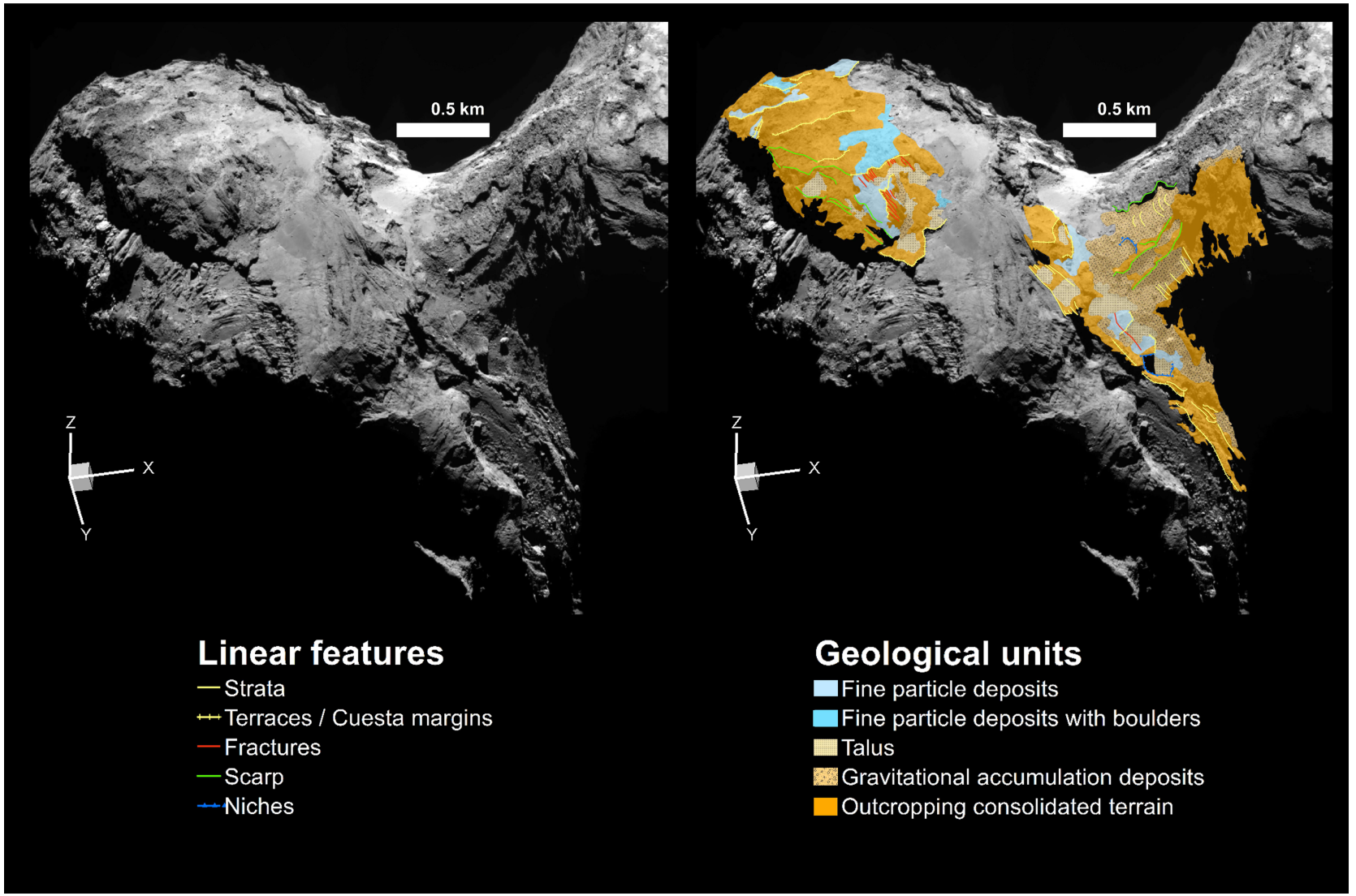

Figure 15. Geomorphological map of Geb, Atum, Sobek and Neith regions.

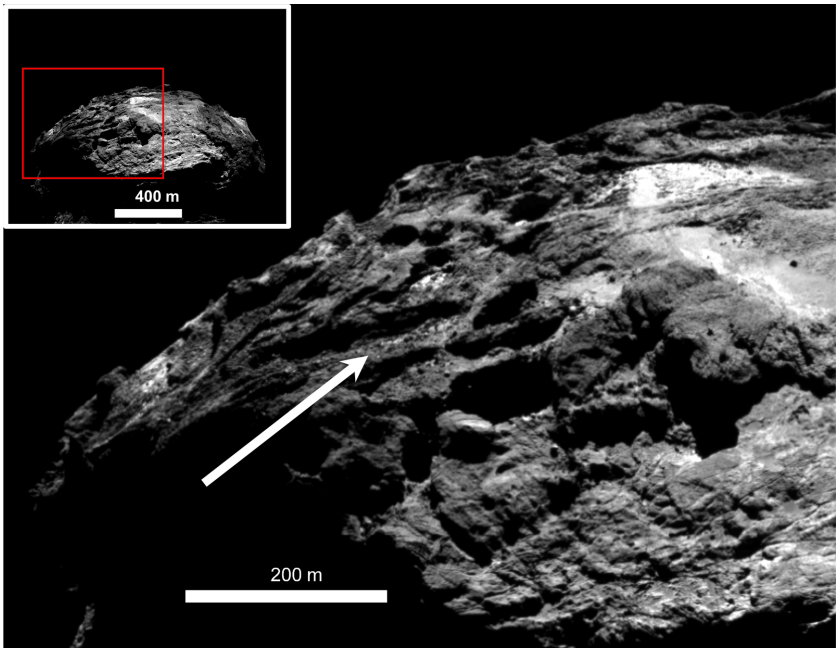

Figure 16. Deposits at the foot of cliffs bounding terrace margins on Wosret.

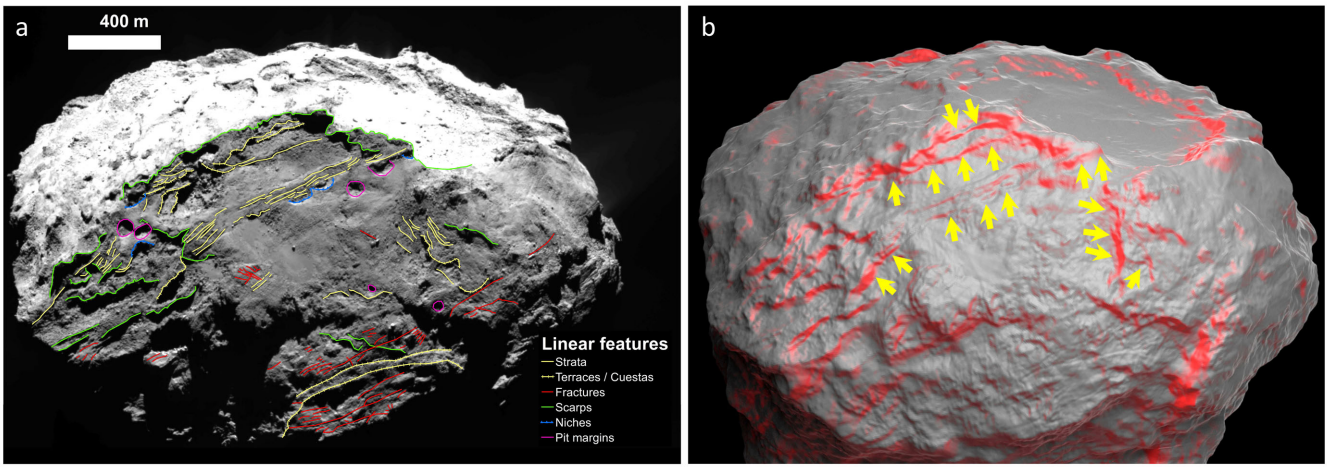

Figure 17. Parallel bands of linear features on the Wosret region can be interpreted as sets of stratification that are being continuous and connected with terraces in a staircase pattern to the left-hand side. (a) The interpretation of linear features in Wosret. (b) The shape model with slopes greater than 35° highlighted in red. Yellow arrows indicate the stratification expressed in the form of parallel bands and aligned terraces.

variegated morphology, whereas in the Southern hemisphere, the irregular landforms seem to have been smoothed away. Finally, the density per unit area of the blocks (#/km^2) in the Southern hemisphere is three times higher than that in the Northern hemisphere (Pajola et al. 2016a). These different morphological characteristics between the two hemispheres could be linked to the different insolation conditions. The Southern hemisphere was strongly heated for 10 month near perihelion, whereas the insolation input for the Northern hemisphere was much weaker because the heliocentric distance is higher at positive sub-solar latitudes. As a result, the erosion rate of the Southern hemisphere should be approximately three times higher than that in the Northern hemisphere (Keller et al. 2015). This could be the reason why the Southern hemisphere is flatter. Indeed, the stronger thermal fatigue and sublimation drives the formation of fractures and a greater production of blocks and boulders (Pajola et al. 2016a), giving rise to more efficient erosive processes on exposed cliffs.

In the dust transport model of Lai et al. (2017), most of the surface of the Northern hemisphere should be covered with dust particles of millimetre to centimetre size, and in every orbit the depth of the new dust cover can reach approximately 60 cm, at least in the Hapi region. This is due to the stronger activity of the Southern hemisphere during perihelion. According to the same model, the fine particle deposits should be scattered and can reach only 10-cm depth in Anhur (Lai et al. 2017). Scattered thin deposits mostly in the Anhur region are exactly what we found and mapped. Hence, the models and observations concur in demonstrating that insolation and airfall mechanisms operate with a diverse intensity on each side of the comet nucleus.

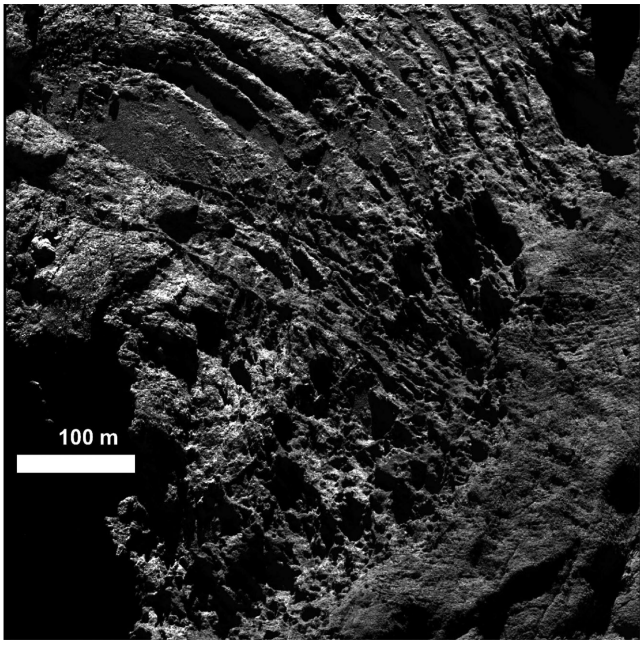

Figure 18. The array of crevices on Khonsu with fine particle deposits inside.

The morphological appearance of the stratification of the Northern hemisphere is quite different from that of the Southern hemisphere. In the former case, the stratification is often shown in the form of wide terraces and cuestas with strata visible on the steeper walls. In the Southern hemisphere, on the other hand, the terraces and cuestas are less extended, and the layering appears more eroded. However, the geological sections interpreted by measuring the strata, terraces and cuestas planes in the Southern hemisphere as well suggest two independent onion-like shells, as in Massironi et al. (2015). However, it is safe to affirm that for further confirmation of such an interpretation of the inner nucleus of 67P, a more robust 3D geological analysis, is required.

5 CONCLUSION

In this work, we realized eight geomorphological maps to investigate the surface textures and structures of the Southern hemisphere of comet 67P in detail by grouping the geological units with common properties that could be formed by the same processes. The outcropping consolidated terrain is the most extensive geological unit in the Southern hemisphere. On the small lobe, the Wosret region is characterized by outcropping consolidated terrain with pervasive fracturing and many scarps and terraces arranged in staircase patterns. At the junction with the neck, the small lobe is dominated by the aligned cliffs of the Neith and Sobek regions. This alignment can be interpreted as the expression of stacks of strata, possibly resulting from accretion of the two lobes. Blocks on the Sobek region may have originated from collapses of nearby cliffs or may have been transported under the influence of the lowest gravity potential in the Southern hemisphere (Lai et al. 2017). The side of the large lobe close to Sobek is represented by the Anhur and Geb regions. These two regions are dominated by outcropping consolidated terrain, but Anhur shows more extensive mass wasting deposits than Geb. The boundary of Anhur and Geb close to Sobek is covered with a thin layer of fine material. This is consistent with the prediction of the global dust transport model in Lai et al. (2017).

The geomorphological maps allowed us to study in detail the surface textures and the possible formation processes of each terrain. Although the Northern hemisphere is characterized by a primary stratification possibly arranged in envelopes, the Southern hemisphere reveals more degraded morphologies and less fine particle deposits. This could be linked to the different insolation conditions and airfall transport between the Northern and Southern hemispheres. As a result, surface geological processes could operate at different intensities on the two hemispheres of the comet nucleus.

ACKNOWLEDGEMENTS

OSIRIS was built by a consortium led by the Max-Planck-Institut fűr Sonnensystemforschung, Göttingen, Germany, in collaboration with Center of Studies and Activities for Space G. Colombo, CISAS, University of Padova, Italy, the Laboratoire d'Astrophysique de Marseille, France, the Instituto de Astrofísica de Andalucía, Consejo Superior de Investigaciones Científicas (CSIC), Granada, Spain, the Research and Scientific Support Department of the European Space Agency, Noordwijk, Netherlands, the Instituto Nacional de Técnica Aeroespacial, Madrid, Spain, the Universidad Politéchnica de Madrid, Spain, the Department of Physics and Astronomy of Uppsala University, Sweden, and the Institut fűr Datentechnik und Kommunikationsnetze der Technischen Universität Braunschweig, Germany. The support of the national funding agencies of Germany (Deutschen Zentrums fűr Luftund Raumfahrt), France (Centre National d'Etudes Spatales), Italy (Agenzia Spaziale Italiana), Spain (Ministerio de Educación, Cultura Deporte), Sweden (Swedish National Space Board; grant no. 74/10:2), and the ESA Technical Directorate is gratefully acknowledged. This work was also supported by grant number NSC102-2112-M-008-013-MY3 and NSC 101-2111-M-008-016 from the Ministry of Science and Technology of Taiwan and grant number 017/2014/A1 and 039/2013/A2 of Science and Technology Development Fund, Macau. We are indebted to the whole *Rosetta* missionteam, Science Ground Segment, and *Rosetta* Mission Operation Control for their hard work making this mission possible.

REFERENCES

Ahnert F. O., 1998, Introduction to Geomorphology. Arnold, London
Auger A.-T. et al., 2015, A&A, 583, A35
Bierman P. R., Montgomery D. R., 2014, Key Concepts in Geomorphology. WH Freeman, San Francisco, CA
Bruno D. E., Ruban D. A., 2017, Planet. Space Sci., 135, 37
Easterbrook D. J., 1993, Surface Processes and Landforms. Macmillan, New York
El-Maarry M. R. et al., 2015a, Geophys. Res. Lett., 42, 5170
El-Maarry M. R. et al., 2015b, A&A, 583, A26
El-Maarry M. R. et al., 2016, A&A, 593, A110
Fairbridge R. W., 1968, Encyclopedia of Geomorphology. Reinhold, New York, p. 1233
Feller C. et al., 2016, MNRAS, 462, S287
Giacomini J. M. et al., 2016, MNRAS, 462, S352
Groussin O. et al., 2015, A&A, 583, A32
Ip W.-H. et al., 2016, A&A, 591, A132
Jorda L. et al., 2016, Icarus, 277, 257
Keller H. U. et al., 2007, Space Sci. Rev., 128, 433
Keller H. U. et al., 2015, A&A, 583, A34
La Forgia F. et al., 2015, A&A, 583, A41
Lai I.-L. et al., 2017, MNRAS, in press
Massironi M. et al., 2015, Nature, 526, 402
Mottola S. et al., 2015, Science, 349, aab0232
Pajola M. et al., 2015, A&A, 583, A37

Pajola M. et al., 2016a, A&A, 592, L2
Pajola M. et al., 2016b, A&A, 592, A69
Preusker F. et al., 2015, A&A, 583, A33
Rickman H. et al., 2015, A&A, 583, A44
Sierks H. et al., 2015, Science, 347, aaa1044
Summerfield M. A., 1991, Global Geomorphology: An Introduction to the Study of Landforms. Addison Wesley Longman, Harlow
Thomas N. et al., 2015a, Science, 347, aaa0440
Thomas N. et al., 2015b, A&A, 583, A17
Thornbury W. D., 1954, Soil Sci., 78, 157
Vincent J.-B. et al., 2015, Nature, 523, 63
Vincent J.-B. et al., 2016, A&A, 587, A14

APPENDIX A: ADDITIONAL FIGURE AND TABLE

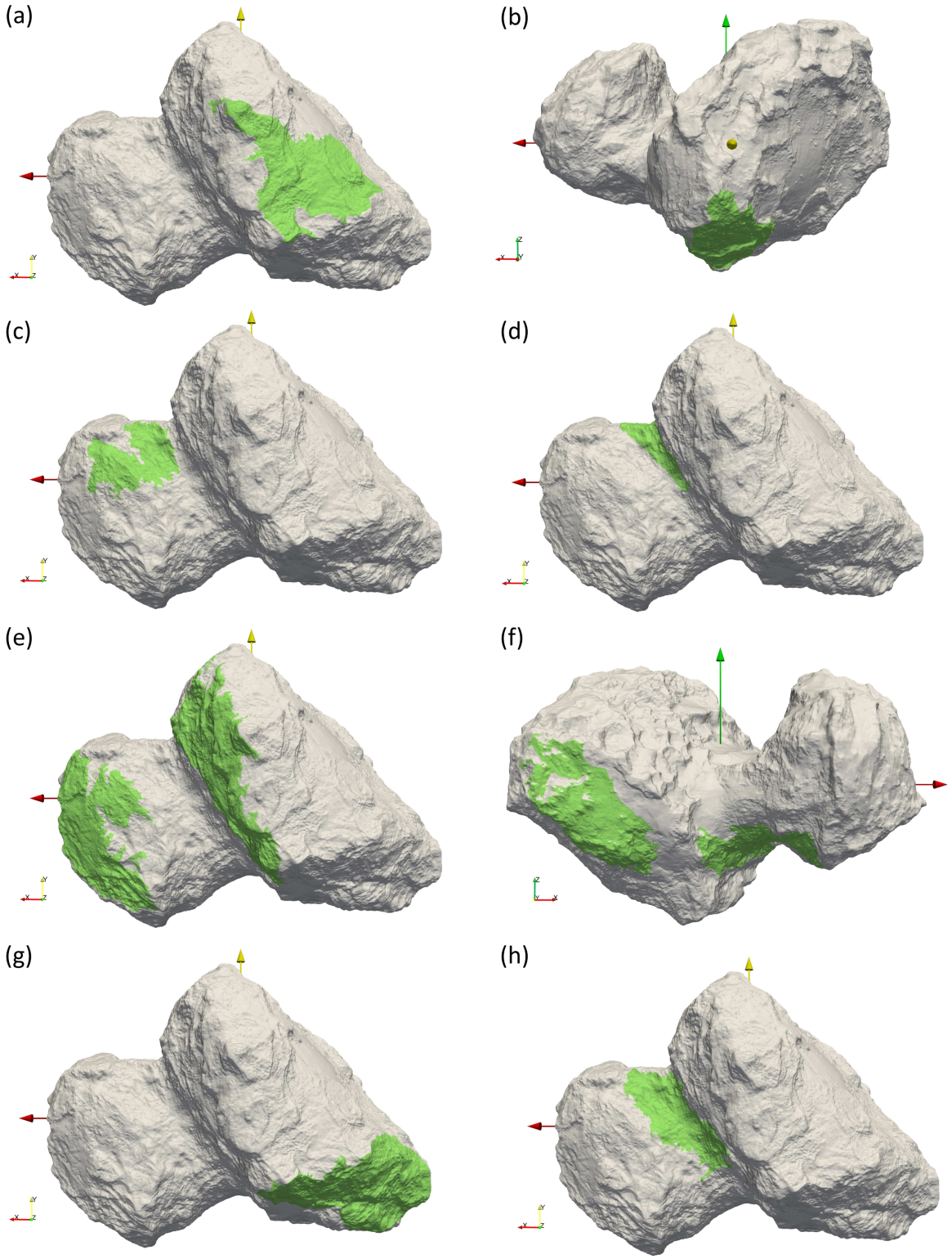

Figure A1. Projection on the shape model of the mapping regions shown in Figs 8–15.

Table A1. The images used in this study.

Figure	ImageID	Distance (km)*	Pixel scale (m)
1a	NAC-2014-08-06T02.43.16.574Z-ID30-1397549100-F22	116.4	2.2
1b	NAC-2014-08-06T06.20.11.419Z-ID30-1397549200-F41	109.7	2.0
1c	NAC-2015-12-12T22.52.06.071Z-ID30-1397549005-F61	101.6	1.9
1d	NAC-2015-12-10T04.31.30.109Z-ID30-1397549002-F41	102.0	1.9
2a	NAC-2016-06-09T20.15.02.728Z-IDB0-1397549700-F22	30.6	0.6
2b	NAC-2016-06-18T03.33.37.444Z-IDB0-1397549300-F22	30.9	0.6
2c	NAC-2015-05-02T06.54.10.576Z-ID30-1397549002-F41	125.1	2.3
3a	NAC-2014-09-21T13.37.34.939Z-IDB0-1397549001-F23	27.6	0.5
3b	NAC-2016-01-27T07.29.19.741Z-IDB0-1397549007-F22	73.1	1.4
4a	NAC-2015-05-02T10.42.52.535Z-ID30-1397549002-F41	124.9	2.3
4b	NAC-2015-06-04T23.56.51.819Z-IDB0-1397549001-F22	208.8	3.9
6a	NAC-2015-05-02T10.42.52.535Z-ID30-1397549002-F41	124.9	2.3
6b	NAC-2015-05-02T06.54.10.576Z-ID30-1397549002-F41	125.1	2.3
6c	NAC-2015-05-02T04.54.10.779Z-ID30-1397549002-F41	125.4	2.3
6d	NAC-2015-05-02T15.09.42.564Z-ID30-1397549002-F41	124.9	2.3
7a	NAC-2015-05-02T07.54.10.586Z-ID30-1397549002-F41	125.1	2.3
7b	NAC-2015-05-02T08.54.10.805Z-ID30-1397549002-F41	125.0	2.3
7c	NAC-2016-01-27T17.20.08.041Z-ID30-1397549000-F22	70.4	1.3
7d	NAC-2015-05-02T12.42.52.621Z-ID30-1397549002-F41	124.8	2.3
8	NAC-2015-05-02T10.42.52.535Z-ID30-1397549002-F41	124.9	2.3
9	NAC-2015-05-02T06.54.10.576Z-ID30-1397549002-F41	125.1	2.3
10	NAC-2015-05-02T04.54.10.779Z-ID30-1397549002-F41	125.4	2.3
11	NAC-2015-05-02T15.09.42.564Z-ID30-1397549002-F41	124.9	2.3
12	NAC-2015-05-02T07.54.10.586Z-ID30-1397549002-F41	125.1	2.3
13	NAC-2015-05-02T08.54.10.805Z-ID30-1397549002-F41	125.0	2.3
14	NAC-2016-01-27T17.20.08.041Z-ID30-1397549000-F22	70.4	1.3
15	NAC-2015-05-02T12.42.52.621Z-ID30-1397549002-F41	124.8	2.3
16	NAC-2015-12-13T01.13.54.451Z-ID30-1397549006-F41	101.0	1.9
17	NAC-2015-05-02T10.42.52.535Z-ID30-1397549002-F41	124.9	2.3
18	NAC-2016-07-16T08.11.12.648Z-IDB0-1397549700-F22	14.1	0.3

*The distance between spacecraft and the centre of comet 67P/C–G.

[1]*Department of Earth Sciences, National Central University, 300 Chung-Da Rd, Chung-Li 32054, Taiwan*
[2]*Department of Geosciences, University of Padova, via G. Gradenigo 6, I-35131 Padova, Italy*
[3]*Center of Studies and Activities for Space G. Colombo, CISAS, 'G. Colombo', University of Padova, Via Venezia 15, I-35131 Padova, Italy*
[4]*Institute of Astronomy, National Central University, 300 Chung-Da Rd, Chung-Li 32054, Taiwan*
[5]*Institute of Space Science, National Central University, 300 Chung-Da Rd, Chung-Li 32054, Taiwan*
[6]*Space Science Institute, Macau University of Science and Technology, Avenida Wai Long,Taipa, Macau*
[7]*Physikalisches Institut der Universität Bern, Sidlerstr. 5, CH-3012 Bern, Switzerland*
[8]*NASA Ames Research Center, Moffett Field, CA 94035, USA*
[9]*Max-Planck-Institut für Sonnensystemforschung, Justus-von-Liebig-Weg 3, D-37077 Göttingen, Germany*
[10]*Department of Physics and Astronomy, University of Padova, Vicolo dell'Osservatorio 3, I-35122 Padova, Italy*
[11]*Laboratoire d'Astrophysique de Marseille, UMR 7326 CNRS & Aix-Marseille Université, 38 rue Frédéric Joliot-Curie, F-13388 Marseille cedex 13, France*
[12]*Centro de Astrobiologia, CSIC–INTA, Torrejon de Ardoz, E-28850 Madrid, Spain*
[13]*International Space Science Institute, Hallerstraße 6, CH-3012 Bern, Switzerland*
[14]*Scientific Support Office, European Space Research and Technology Centre/ESA, Keplerlaan 1, Postbus 299, NL-2201 AZ Noordwijk ZH, the Netherlands*
[15]*Department of Physics and Astronomy, Uppsala University, Box 516, SE-75120 Uppsala, Sweden*
[16]*PAS Space Research Center, Bartycka 18A, PL-00716 Warszawa, Poland*
[17]*Institut für Geophysik und extraterrestrische Physik (IGEP), Technische Universität Braunschweig, Mendelssohnstr. 3, D-38106 Braunschweig, Germany*
[18]*Department of Astronomy, University of Maryland, College Park, MD 20742-2421, USA*
[19]*Akademie der Wissenschaften zu Göttingen, Geschäftsstelle, Theaterstraße 7, D-37073 Gottingen, Niedersachsen, Germany*
[20]*LESIA – Observatoire de Paris, CNRS, Université Pierre et Marie Curie, Universite Paris Diderot, 5 place J. Janssen, F-92195 Meudon, France*
[21]*INAF, Osservatorio Astronomico di Padova, Vicolo dell'Osservatorio 5, I-35122 Padova, Italy*
[22]*CNR – IFN UOS Padova LUXOR, Via Trasea, 7, I-35131 Padova, Italy*
[23]*Department of Physics and Astronomy, Uppsala University, Box 516, SE-75120 Uppsala, Sweden*
[24]*Department of Industrial Engineering, University of Padova, via Venezia 1, I-35131 Padova, Italy*
[25]*University of Trento, Via Mesiano 77, I-38100 Trento, Italy*
[26]*INAF – Osservatorio Astronomico, Via Tiepolo 11, I-34014 Trieste, Italy*
[27]*Instituto de Astrofísica de Andalucía (CSIC), Glorieta de la Astronomìa, E-18008 Granada, Spain*
[28]*Deutsches Zentrum für Luft- und Raumfahrt (DLR), Institut für Planetenforschung, Rutherfordstraße 2, D-12489 Berlin, Germany*
[29]*Operations Department, European Space Astronomy Centre/ESA, P.O.Box 78, E-28691 Villanueva de la Canada, Madrid, Spain*
[30]*Department of Information Engineering, University of Padova, Via Gradenigo 6/B, I-35131 Padova, Italy*

This paper has been typeset from a TEX/LATEX file prepared by the author.